IEEE Access
Multidisciplinary ⋮ Rapid Review ⋮ Open Access Journal

Received 8 June 2023, accepted 30 June 2023, date of publication 4 July 2023, date of current version 11 July 2023.

Digital Object Identifier 10.1109/ACCESS.2023.3292307

RESEARCH ARTICLE

Multi-Objective Hybrid Optimization Algorithm for Design a Printed MIMO Antenna With n78–5G NR Frequency Band Applications

VAHID HOSSEINI HASBESTAN[1], YOUSEF FARHANG[2], KAMBIZ MAJIDZADEH[1], AND CHANGIZ GHOBADI[3]

[1]Computer Engineering Department, Urmia Branch, Islamic Azad University, Urmia 57169-63896, Iran
[2]Department of Computer Engineering, Khoy Branch, Islamic Azad University, Khoy 15847-15414, Iran
[3]Department of Electrical Engineering, Urmia University, Urmia 57179-44514, Iran

Corresponding author: Yousef Farhang (yfarhang@yahoo.com)

ABSTRACT This study introduces a novel multi-objective optimization algorithm integrating Customized Mutated Particle Swarm Optimization (CM-PSO) and an innovative modified Genetic Algorithm (GA) using an unexplored merged chaotic map. The hybrid algorithm converges to desired results faster than CM-PSO and modified GA without trapping in local minima. Validation is conducted by designing a single-element and simple-structure dipole antenna so that its optimized S_{11} is better than -30 dB at the resonance frequency and covers the 3.3 to 3.8 GHz frequency band with $S_{11} < -10$ dB. Certainly, the -30 dB and covering frequency band criteria can be modified in the proposed algorithm. In the algorithm, the isolation between elements of a quad-Multiple-Input/Multiple-Output antenna, constructed using optimized dipole antennas, is set to be less than -20 dB (changeable criteria) so that the smallest size can be achieved. Computer Simulation Technology (CST) Studio Suite carries out electromagnetic and high-frequency simulations, and the novel developed optimization algorithm in MATLAB determines what and how much parameter values need to be changed by CM-PSO or an innovative modified GA in order to enhance the antenna's S_{11} result and its Impedance Bandwidth (IBW). The input parameters of the algorithm are the dimensions of the proposed antenna's elements, which significantly influence its performance.

INDEX TERMS Chaotic map, CM-PSO algorithm, dipole antennas, genetic algorithm, hybrid optimization algorithms, MIMO antennas, printed antennas.

I. INTRODUCTION

One of the most crucial endeavors has always been optimizing engineering systems' design [1]. An inexact trial and error method is one of the most commonly used optimization techniques, which is unsuitable for intricate designs due to the increased number of parameters involved. In order to optimize sensitive and complicated engineering systems precisely, investigators have developed algorithms based on computer code [2]. Telecommunication systems are one of the available engineering systems which cover numerous human beings' daily social connections, work, and activities. Antennas are an inevitable part of modern telecommunication systems [3], [4]. Therefore, optimizing antennas' scattering and radiation parameters make it possible to achieve the best performance for telecommunication systems [5]. However, optimization techniques are mainly categorized into meta-heuristic and deterministic techniques [6]. Over the last few years, there has been an increase in demand for systems with high data transfer speeds, capacities, and reliability. Meanwhile, Multiple-Input/Multiple-Output (MIMO) antennas are considered a suitable choice for these systems. MIMO systems increase in capacity as the number of elements increases according to Shannon's law. As a result of MIMO antennas, multipath interference fading has been eliminated, and their reliability has improved. The MIMO antenna is designed by designing radiation elements individually, then by putting these elements together in the next step [7]. Today, printed

The associate editor coordinating the review of this manuscript and approving it for publication was Bilal Khawaja.

This work is licensed under a Creative Commons Attribution-NonCommercial-NoDerivatives 4.0 License.
For more information, see https://creativecommons.org/licenses/by-nc-nd/4.0/

antennas have become more popular due to their light structure, cheapness, and ease of connection to other microwave components [8], [9], [10], [11], [12], [13], [14], [15]. One of the most critical challenges in designing an antenna is choosing its optimal physical parameters to achieve proper antenna performance. Nowadays, optimization methods based on algorithms gained special attention due to their high speed and accuracy.

A deep neural network (DNN) concept is used to calculate the operating frequency band of an E-shape Patch Antennas (ESPAs) in [16]. The applied neural network model is accomplished on a 5-layer framework cooperating with an adaptive learning rate algorithm using a simulated database of 144 ESPAs. The 144 ESPAs employ multiple geometric and electrical parameters to create a database for model training in terms of resonance frequency. The proposed model is optimized by employing the K-fold cross-validation scheme in the training stage. The model of the proposed algorithm is trained on 130 dataset numbers with an Average Percentage Error (APE) of 0.269 between intended and simulated values. In this design, an E-shaped patch antenna, including two slits fed by coaxial cable, has been analyzed and investigated so that several geometrical and electrical parameters are inputs of the algorithm, and the antenna's resonant frequency is the output of the algorithm. A new hybrid optimization method based on Differential Evolution (DE) and Naked Mole-Rat (NMR) algorithms is reported in [17] for microstrip antenna design optimization. The proposed technique solves the problems of local optima traping and poor exploration concerns of DE and basic NMR versions. The innovation of this work is the use of Levy-based scaling and simulated annealing-based mating factors to accomplish the algorithm. The proposed antenna in this study is a simple monopole antenna printed on an FR4 substrate, and by employing two inverted U-shaped slots on the patch and two C-shaped strips close to the feed line, the rejection characteristics are achieved. The proposed algorithm reduces antenna size, and three notches have also been obtained with the coverage to an ultra-wide frequency band. A new hybrid algorithm is proposed in [18] for pattern synthesis of conformal phased array antennas. In the first step, this work presents an improved genetic algorithm (IGA) and an improved particle swarm optimization (IPSO) algorithm to solve the problems of the traditional genetic and particle swarm optimization algorithms. In the second step, a hybrid algorithm composed of IGA and IPSO named HIGAPSO is introduced based on the grafting concept in botany. The mentioned stacked array antenna comprises microstrip patch elements exciting with coaxial cables. The measured results approve that the proposed algorithm can achieve the optimum design for the array. Also, an artificial intelligence AI-driven antenna design optimization algorithm is investigated for a slot array antenna to broaden the impedance bandwidth (IBW) [19]. The slot array consists of a sequential rotated feeding network, four grounded substrates, and four-element antennas. The proposed AI-driven antenna design technique optimizes the feeding network with multiple related design parameters to find the broadest Bandwidth (BW).

In [20] a three-element mesh Yagi-Uda antenna is discussed. This wired antenna has been configured randomly in order to achieve the optimal Front-to-Back Ratio (FBR), radiation pattern, and beamwidth (BW) using PSO and genetic algorithms. Utilization of computer software can also be employed to design an accurate fractal antenna [21]. This study aims to provide an effective methodology for designing a miniaturized antenna and its construction. With the aid of several optimization algorithms including particle swarm optimization, weed invasion optimization, and genetic algorithms, the conformal array antennas' radiation pattern has been optimized.

Optimizing electromagnetic structures is achieved by combining PSO and GA techniques. Coupling is primarily used to reduce the drawbacks of the traditional GA method. Two linear and circular arrays were successfully designed by the proposed method. Arrays with 10 and 31 elements were used for linear and circular arrays, respectively. The modified Bernstein polynomial was also employed during the analysis in order to minimize the number of variables [22]. There is a discussion in [23] regarding the optimization of a bowtie antenna that operates in three frequency bands based on two optimization techniques, PSO and GA. In addition to improving antenna results by utilizing both the PSO and GA optimization methods, it was possible to obtain lower frequencies by utilizing both optimization techniques without adding additional components. Using both PSO and GA, the optimized antenna's radiation patterns were close to those of the original antenna. When PSO was used, there were 8 iterations in total.

This study combines Customized Mutated Particle Swarm Optimization (CM-PSO) [24] and a customized version of classic Genetic Algorithms (GA), Augmented-GA (AGA), using a novel Merged Chaotic Map (MCM) to design an antenna with optimized characteristics, Fig. 1. It has been pointed out in [24] that CM-PSO has the ability to approach promising results for the antenna design. However, the Chebyshev Chaotic Map (CCM) is also utilized to modify the classical GA and enhance its performance in approaching final results. In order to combine CM-PSO and AGA, a novel chaotic map ingeniously is introduced using Sinusoidal (SCM), Iterative (ICM), and Piecewise (PCM) Chaotic Maps. Consequently, the CM-PSO and AGA functionalities are independent and easy to handle. A set of Benchmark Functions (BFs) are employed in [25] to successfully evaluate the effectiveness of the proposed algorithm by simulations, including the Rastrigin Function (RaF), Ackley Function (AF), Rosenbrock Function (RoF), and Booth Function (BoF). A further benefit of the mentioned research is that it validates its efficacy in solving electromagnetic problems as well. Consequently, it must be noted that such a combination of algorithms improved the antenna's elec-

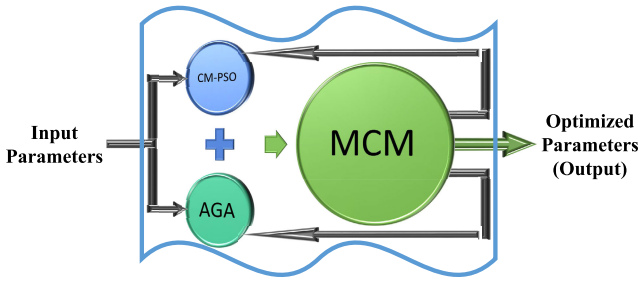

FIGURE 1. Multi-objective hybrid optimization algorithm.

tromagnetic properties performance. Therefore, to show the algorithm's effectiveness in solving electromagnetic problems and antenna design, cost functions, Eqs. (1), as shown at the bottom of the next page, and (2), are defined to test the performance of the used algorithm. During the optimization process, minimizing the defined cost functions are the primary goal which means adjusting and improving the antenna's performance with the desired predefined characteristics. Therefore, the developed algorithm tunes the proposed simple-structure dipole antenna's parameters (length and width of the antenna's different sections) to acquire -30 dB predefined resonance intensity at 3.5 GHz frequency in this approach. Furthermore, the physical parameters should be adjusted so that IBW covers the n78 - 5G NR frequency band applications, 3.3 to 3.8 GHz.

II. SYSTEM MODEL

The main goal of the investigation is to enhance the antennas' performance by modifying the physical dimensions of their elements and employing a novel multi-objective hybrid algorithm based on CM-PSO, MCM, and AGA. Accordingly, introducing additional optimization algorithms can potentially speed up the optimization process's convergence. Certainly, combining multiple algorithms, each with its own strengths and weaknesses can exploit their complementary characteristics to improve overall optimization performance, including accelerating convergence and reducing the number of iterations required to find an optimal solution. It may, however, add more complexity to the proposed hybrid multi-objective optimization algorithm. The MATrix LABoratory (MATLAB) simulator software is used to develop the mentioned hybrid algorithm and then integrated into Computer Simulation Technology (CST) Studio Suite to conduct antenna design processes. Next, a low-profile printed dipole antenna is suggested in the first phase to improve its performance by the proposed algorithm to validate its functionality. Therefore, its S_{11} is improved in the CST simulator software using the mentioned algorithm in which S_{11} at $f_r = 3.5$ GHz resonance frequency is less than a predefined criterion, in this study -30 dB, and covers the frequency band of 3.3 to 3.8 GHz (BW). Indeed, Ω_1 cost function in Eq. 1 is defined, in which decision variables L_d, W_d, L_g, W_g, and L_3 are parameters of the proposed antenna for applying adjustment by the suggested algorithm. It is worth noting that acquiring the antenna's optimized parameters and gaining maximum performance is tiresome just by means of CST or High-Frequency Structure Simulator (HFSS) simulator software.

In the next stage of the construction process, the isolation characteristic of a quad-port MIMO antenna is ingeniously adjusted by the formed optimization algorithm, assessed for validation in CST simulation software, and fabricated and tested after verifying the simulation outcomes. For this aim, the isolation (S_{mn}) criteria between parallel and perpendicular antenna elements are set to be less than -20 dB. Strictly, such a cost function, Ω_2, for this phase is defined as:

$$\begin{aligned} \Omega_2 = \min_{f,d_1} & \begin{cases} d_1\ [mm] \\ |S_{mn}(IBW, d_1)| - 20\ [dB] \end{cases} \\ \text{Subject to:} \quad & IBW = [3.3, 3.8]\ [GHz] \\ & 40\ [mm] \le d_1 \le 50\ [mm] \end{aligned} \tag{2}$$

in which decision variable d_1 is minimum distance between parallel and orthogonal antennas. Finally, the proposed MIMO antenna is fabricated after adjusting the mentioned distance to get desired isolation. As a result of the fabrication of the antennas, the experimental results corroborate the performance of the implemented optimization algorithm. Accordingly, the proposed hybrid optimization algorithm can optimize complex antennas with minor modifications to its input and output arguments.

III. DEVELOPING MULTI-OBJECTIVE HYBRID OPTIMIZATION ALGORITHM USING CM-PSO ALGORITHM, MERGED CHAOTIC MAP, AND AUGMENTED-GENETIC ALGORITHM

According to the [24], a classical PSO algorithm is modified, CM-PSO, to escape from trapping in local minima and approach the global one at the fastest possible paces in complex engineering design problems. Consequently, its ability is validated by a monopole antenna design in which the related resonance frequency is adjusted to the desired frequency band. However, combining other algorithms can improve the proposed algorithm's convergence rate, Fig. 2. Fig. 2 presents the rate of algorithms to converge proper S_{11} intensity to design the proposed dipole antenna in section IV.

Concerning establishing a hybrid algorithm using a CM-PSO and extended-GA, the CCM (Fig. 4a and Eq. (6)) is utilized instead of a random function in the classical GA to generate the main generations (parents) of the populations/researchers/agents. Moreover, novel masks (α) are generated utilizing a fraction of the same chaotic map, CCM, and applied to generate a new set of offspring in the arithmetic crossover.

$$\boldsymbol{\alpha} = (\alpha_1, \alpha_2, \ldots, \alpha_q), \quad -\frac{CCM_i}{h} \le \alpha_i \le \frac{CCM_i}{h} + 1 \tag{3}$$

in which q is the number of paired parents. In this study, h is set to 10 regarding simulation results. In this way, offsprings

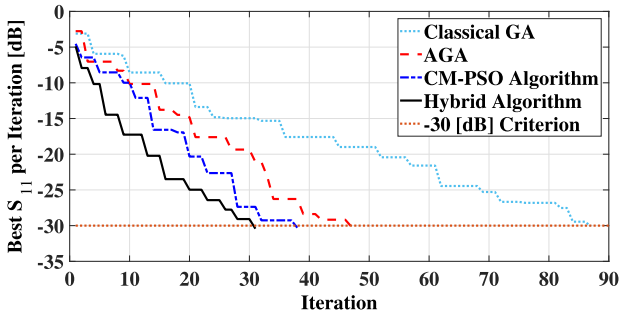

FIGURE 2. The rate of algorithms approaching a proper S_{11} depth with 40 populations/researchers.

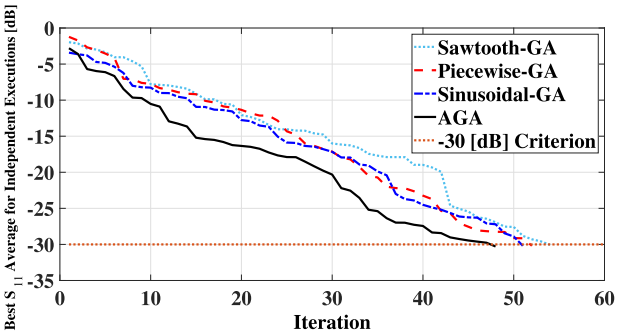

FIGURE 3. The average rate of extended GAs approaching a proper S_{11} intensity with 40 populations/researchers.

have the opportunity to be better than their parents, avoid trapping in local points, and find global ones. However, the values of the decision variables should be checked not to overflow or underflow from the maximum and minimum limits, respectively. Furthermore, the mutation rate (μ) is set to a fraction of the CCM, which determines the length of the pace (σ) in each Number of Function Evaluations (NFE):

$$\sigma = \mu(Boundary_{Max.} - Boundary_{Min.}), \quad \mu = \frac{CCM_{NFE}}{h} \tag{4}$$

where $[Boundary_{Min.}, Boundary_{Max.}]$ are boundaries of the decision variables, which can be found in Eq.s (1) and (2). Then, the mutation intensity can vary in each NFE which avoids trapping in local points. It has to be noted that chaotic maps can generate pseudorandom numbers between [0, 1], which means the random numbers have a generation pattern and are reproducible/repeatable. In this study, the first input of the CCM is set to $x_{CCM_1} = 0.7$ pseudorandomly. Chaotic maps are indeed sensitive to their initial values. In chaos theory, small differences in initial conditions can lead to significantly different outcomes in the long term, known as the ''butterfly effect''. In fact, different initial values for chaotic maps may lead to different solutions if the optimization problem is non-convex and has multiple local optima, which is not fruitful for this study at the desired bandwidth. Moreover, the utilized chaotic maps have repeatable patterns and thus minimize the effect of initial values on the final convergence results. However, some simulations are applied, and considering the characteristics of the optimization problem, the computational resources available, and the trade-off between computational time and solution quality when deciding on the appropriate approach, initial values are set. Therefore, in this way, one can neglect the effect of a random number in population generation, arithmetic crossover, and mutation in independent explorations and exploitations and just concentrate on the effect of the modified GA algorithm on the proposed hybrid algorithm's results. Also, chaotic maps generate smoother pseudorandom numbers, usually with small jumps. Consequently, it causes a smaller boxplot for the adjusted parameters and optimized results in independent executions which means reliability in smaller NFE counters, Figs. 5, 9, 14(c), and 14(d). Moreover, Fig. 2 presents that the mentioned technique can also improve the convergence rate of the classical GA, which is a positive characteristic for complex antenna design problems. It should be mentioned that different chaotic maps are evaluated in combination with classical GA, such as Sawtooth, Sinusoidal, Piecewise, and Chebyshev. However, the highest convergence rate is obtained using the CCM in independent executions (simulations), named Augmented-GA (AGA). In order to determine the average convergence rate, 10 independent optimizations are performed, Fig. 3.

Concerning the combination issue, the CM-PSO and AGA should be combined easily and ingeniously in a way that would increase the final hybrid algorithm's convergence rate and make it straightforward to control the optimization process. For this aim, a novel MCM is introduced to combine the mentioned algorithms, Eq. (5), as shown at the bottom of page 6, and Fig. 4(b), and a threshold value is set to decide which algorithm tries to find global minimum points in the design problem during the optimization process. Undeniably, the MCM threshold value is employed to determine the CM-PSO or AGA to continue the optimization process independently, making combining algorithms easier and avoiding

$$\begin{aligned} \Omega_1 = \min_{L_d, W_d, L_g, W_g, L_3, f_r} & \begin{cases} f_r(L_d, W_d, L_g, W_g, L_3) - 3.5\ [GHz] \\ |S_{11}(f_r)| - 30\ [dB] \end{cases} \\ \text{Subject to:} \quad & S_{11}(IBW) \le -10\ [dB] \\ & IBW = [3.3, 3.8]\ [GHz] \\ & [9, 30, 9, 25, 1]\ [mm] \le [L_d, W_d, L_g, W_g, L_3] \le [10, 40, 12, 45, 3]\ [mm] \end{aligned} \tag{1}$$

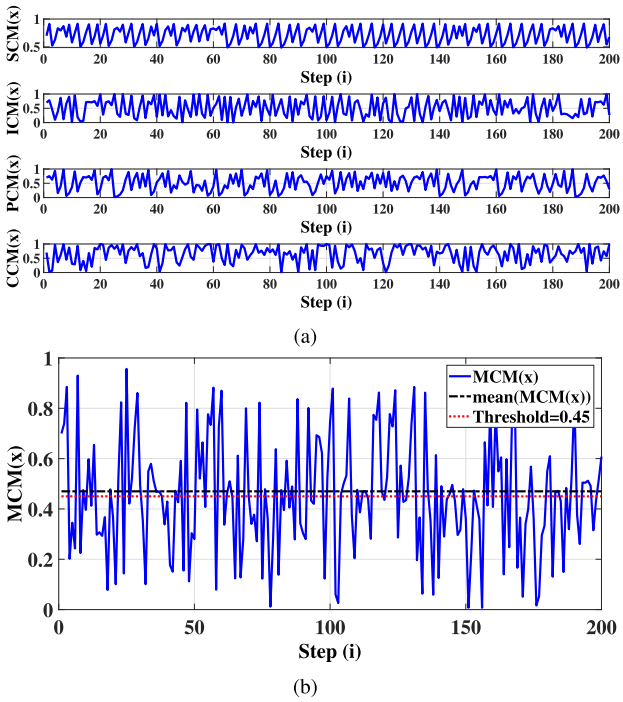

FIGURE 4. Chaotic maps for 200-time steps: (a) Presents the CCM, PCM, ICM, and SCM, respectively, and (b) Presents the MCM, its mean value (0.47), and threshold criterion.

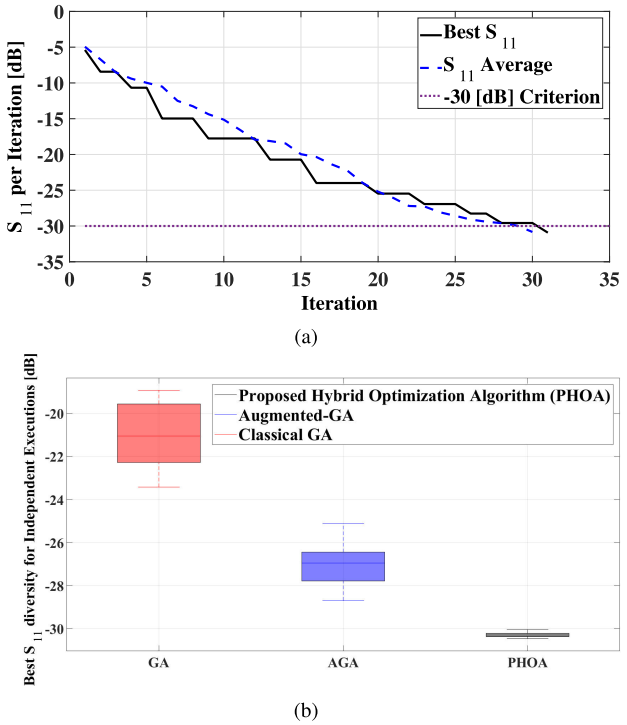

FIGURE 5. S_{11} convergence rate and boxplot: (a) The S_{11} convergence and average S_{11} convergence for the proposed hybrid algorithm, and (b) The boxplot of S_{11} for GA, AGA, and multi-objective hybrid optimization algorithms.

tiresome formula combinations. In this study, the CM-PSO algorithm will be utilized for optimization if the MCM value exceeds the threshold. Otherwise, the AGA will be deployed to find global minima points in the design problem. The proposed MCM generates pseudorandom numbers between 0 and 1 with a 0.47 mean value (for more than 3000 times steps) and a repeatable pattern in individual executions. Simulation results approve that determining 0.45 as a threshold gives better solution results in less NFE for the cost function. It means the CM-POS algorithm is better suited to perform most of the optimization. Indeed, simulation results prove that the CM-PSO algorithm has a faster pace to approach the final results in fewer iterations considering the AGA, Fig. 2. Due to this fact, the authors believe that a threshold less than and closer to the mean value of the MCM gives a better solution for the design problem. Based on the values of the threshold criteria applied to simulation studies, this idea has been evaluated and approved. As a result of simulation results, it is found that the hybridization property makes the hybrid algorithm more likely to avoid stocking in local minima and approach the global minimum.

Different chaotic maps are combined and used to introduce a new MCM and unite the AGA and CM-PSO algorithms. Regarding the independent simulation results, however, it seems that innovatively combining Sinusoidal (Eq. (9)), Iterative (Eq. (8)), and Piecewise (Eq. (7)), as shown at the top of page 11) chaotic maps (Fig. 4(a)) avoids more complexity of the proposed one and evades trapping in local minima. Easily, the average of the SCM and ICM chaotic maps is obtained when their input arguments are respectively calculated using ICM and PCM chaotic maps, named Merged Chaotic Map (MCM), Eq. (5). In this study, the first input of the MCM is set to $x_{MCM_1} = 0.7$ pseudorandomly. This argument can be changed to modify the mean and, consequently, the threshold of the MCM to determine which optimization algorithm should be utilized, which directly affects the convergence rate, Eq. 5.

Figure. 5(a) presents the convergence rate of the S_{11}, including its average for agents/researchers. It is proven by the figure that all researchers/agents are converging to -30 dB around 30 iterations. In Fig. 5(b), boxplots of the S_{11} results for the proposed dipole antenna are computed using 40 iterations and 40 populations/researchers for GA, AGA, and the newly proposed algorithm. It indicates that GA could not achieve a proper S_{11} regarding the number of iterations and populations with a high range of variation from -23.43 to -18.92 dB. Also, AGA gave better results compared to GA with the same conditions and smaller variations from -28.71 to -25.12 dB. In fact, the proposed hybrid algorithm touched the final target with a small deviation of -30.47 to -30.05 dB.

Simulation results, Figs. 2 and 5, prove that the proposed multi-objective hybrid optimization algorithm prevents overstocking in local minima and approaches global ones more expeditiously and reliably. In Fig. 6, the operational details of the proposed algorithm are presented. As can be seen in Fig. 6, the populations and researchers are generated and initialized by algorithms. After evaluating the cost functions

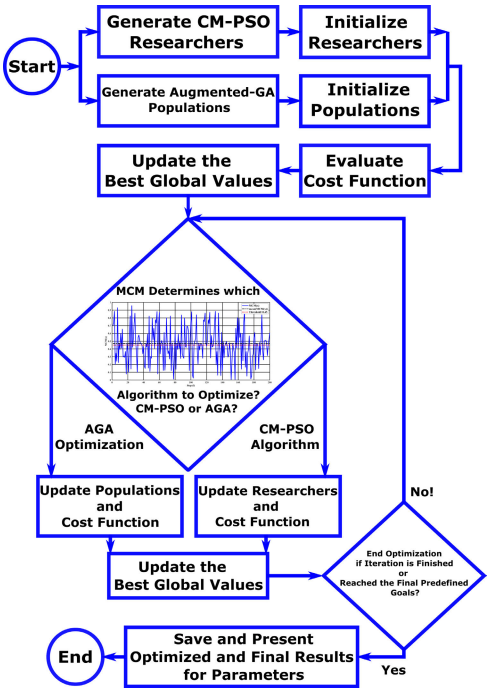

FIGURE 6. Functionality flowchart and decision making of the proposed Multi-Objective Hybrid Optimization algorithm.

for each phase of the dipole antenna/quad-MIMO dipole antenna structure design, the best position is determined based on minimal cost functions. A novel MCM chooses which algorithm to start or continue the optimization process based on the threshold value. Afterward, the positions of the populations/researchers are updated, and cost functions are evaluated as a result of the updated positions. Minimal cost functions are once again used to determine the best position. Finally, based on the predetermined conditions, the developed algorithm decides whether to save and indicate the optimized and final parameters or to return and continue optimizing. Table 1 compares the algorithms and antennas proposed in the literature with this approach, which illustrates one of the fastest convergence rates.

IV. PHASE ONE: DESIGNING A SIMPLE-STRUCTURE PRINTED DIPOLE ANTENNA FOR THE N78 - 5G NR FREQUENCY BAND

This study presents an antenna for indoor micro-BTS applications with the n78 - 5G NR Frequency Band. Indeed, the designed single-element antenna is a simple-structure printed dipole antenna. This antenna is printed on an FR4 substrate with a dimension of $60\times60\times1.6$ mm^3, a 0.02 loss-tangent, and a 4.3 relative permittivity. The dipole arms and ground plane used under the radiation element in this antenna have rectangular- and trapezoidal-shaped. The length of the dipole

TABLE 1. Comparing the characteristics of algorithms and antennas of other articles in literature with the proposed method and antenna (DNN, DE, NMR, IGA, IPSO, MGA, and TS stands for Deep Neural Network, Differential Evolution, Naked Mole-Rat, Improved GA, Improved PSO, Modified Ga, and This Study, respectively.

Ref.	Antenna Type	Algorithm	Complex or Simple	Iteration Number	Pop. or Agents
[16]	E-shaped patch	DNN	Complex	–	–
[17]	Patch	DE NMR	Complex	500	60 51
[18]	Conformal antenna array	IGA IPSO	Complex	2000	32
[24]	Monopole MIMO	CM-PSO	Simple	25–30	100
[25]	Monopole	MCM CM-POS MGA	Simple	25–30	100
TS	Dipole MIMO	MCM CM-PSO AGA	Simple	25–30	40

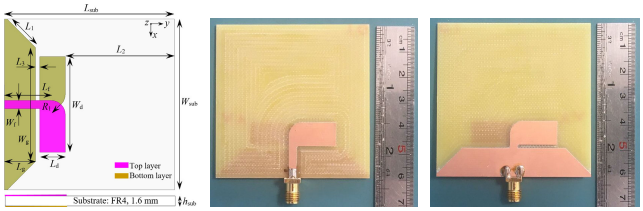

(a) (b) (c)

FIGURE 7. The proposed dipole antenna geometry: (a) Front- and back-view of the schematic microstrip-fed dipole antenna, (b) Front-view of the fabricated dipole antenna, and (c) Back-view of the fabricated dipole antenna.

TABLE 2. Invariable sizes of the offered dipole antenna.

Parameter	Size [mm]	Parameter	Size [mm]
L_{sub}	60	W_{sub}	60
W_f	2.8	R_1	7.5
h_{sub}	1.6	-	-

arm (W_d) is approximately equal to the half wavelength of the resonance frequency, and the length and width of the microstrip transmission line, L_f and W_f, are selected in a way to match the impedance of 50 Ω. Figure 7(a) illustrates the schematic design of the proposed printed dipole antenna. The invariable sizes of the designed antenna are displayed in Table 2. An incomplete ground plane is the most typical approach to enhance microstrip antenna performance, which

$$MCM_j(x_{MCM_{j-1}}) = x_{MCM_j} = \frac{SCM_j\left(ICM_j(x_{MCM_{j-1}})\right) + ICM_j\left(PCM_j(x_{MCM_{j-1}})\right)}{2} \quad (5)$$

is utilized in this study, as shown in Fig. 7. A gap between the ground plane and radiating element is utilized to raise the effective inductance and capacitance on the complete equivalent electrical circuit of the proposed antenna. The mentioned gap significantly influences the antenna's IBW and radiation properties. However, more smallish ground plane height reduces the cross-polarization level. The cross-polarization pattern improves considerably by increasing ground plane height since it delivers additional resonant modes, and the increased current on the ground plane partially contributes to the total radiated field.

The dipole arms are fed using a coaxial cable in which a microstrip line is responsible for transmitting the signal from the input to the radiant elements. L_d, W_d (length and width of the dipole), L_g, W_g (length and width of the truncated ground), and L_3 (the gap between dipole and truncated ground) are the most critical design parameters of the antenna, and each can have a significant impact on its performance. Therefore, analyzing these parameters and selecting their optimized values seems necessary. One of the well-known methods for this effort is the parametric analysis method in CST and HFSS simulator software. In this method, the optimal value for the desired element is selected by changing the size of one parameter and keeping the size of other elements constant. However, one of the significant drawbacks of this method is that it takes much time and cannot analyze all antenna parameters simultaneously. Consequently, it can be claimed that the optimal values obtained in this method are not absolute, and by performing further analysis or changing the order of the analyzed parameters, different optimal values can be obtained. Thus, this method is unlikely to produce final and absolute values.

Therefore, an algorithm-based optimization method can enhance the analysis time and hardware consumption. Accordingly, L_d, W_d, L_g, W_g, and L_3 can be considered as the main input parameters of the developed multi-objective hybrid algorithm to adjust IBW and improve the resonance intensity of the offered dipole antenna. The proposed algorithm is developed using MATLAB. As a result, MATLAB is integrated with CST to control and carry out simulations that achieve the desired results. Undoubtedly, electromagnetic and high-frequency simulations are done by CST, and the developed algorithm decides what and how much to change input parameters by which algorithm, CMPSO or AGA, regarding the antenna's S_{11} result and IBW. Consequently, to achieve the final results in the briefest time and rerun the proposed algorithm several times to evaluate its reliability, the algorithms' objectives are set to achieve a S_{11} of more than -30 dB at the resonance frequency and covering 3.3 to 3.8 GHz frequency band with $S_{11} < -10$ dB. Consequently, the adjusted sizes for the determined parameters are derived by MATLAB simulator software based on the proposed hybrid algorithm, Table 3. Eventually, CST and Advanced Design System (ADS) software are used to extract the details of the antenna's PCB layout and fabricate it.

TABLE 3. Adjusted sizes of the antenna's decision variables by the optimization algorithm.

Parameter	Size [mm]	Parameter	Size [mm]
L_d	9.03	W_d	35.55
L_g	10.95	W_g	39.98
L_3	1.50	-	-

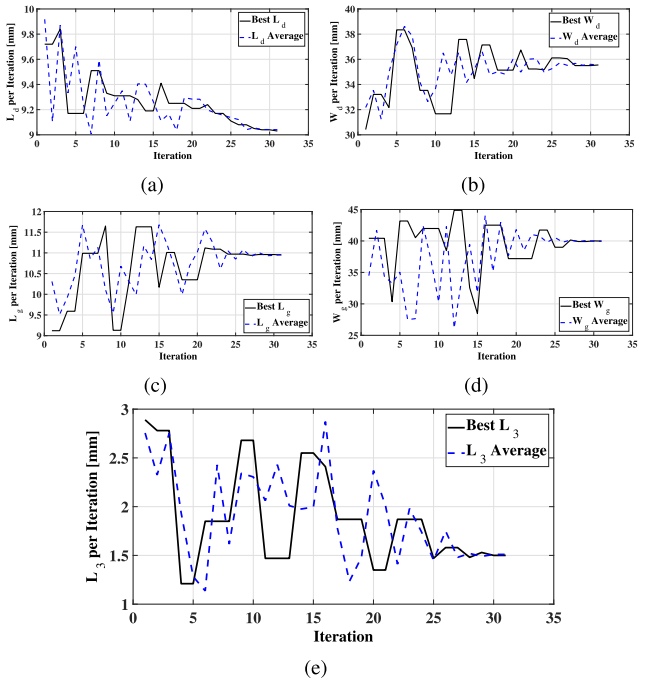

FIGURE 8. Convergence rate of decision variables using the proposed hybrid algorithm: (a) Approaching L_d to its final value, (b) Approaching W_d to its final value, (c) Approaching L_g to its final value, (d) Approaching W_g to its final value, and (e) Approaching L_3 to its final value.

Figure 8 presents the convergence rate and approaching the final goals for the decision variables. The results are obtained for 40 agents/researchers. As is evident from the results, the final goals are attained after around 27 iterations. Regarding the average convergence rate results, all researchers/agents concentrate on the final target.

The boxplots of the decision variables for 40 agents/researchers, about 30 iterations, and 10 independent executions are presented in Fig. 9 to show the reliability of the proposed hybrid algorithm. Results prove that the proposed algorithm gives the most reliable results comparing GA and AGA. There is no doubt that more iterations will produce more accurate results, which means more reliability.

The comparisons of simulated and tested results of the proposed single-element antenna are provided in Fig. 10 and 11. As shown in Fig. 10, the simulated S_{11}'s magnitude by CST simulator software for the suggested simple-structure dipole antenna is -31.5 dB strictly at 3.5 GHz frequency. The measured S_{11}'s magnitude is -30.43 dB around the resonance frequency, which has an understandable discrepancy from the simulated ones. According to the measured results, the

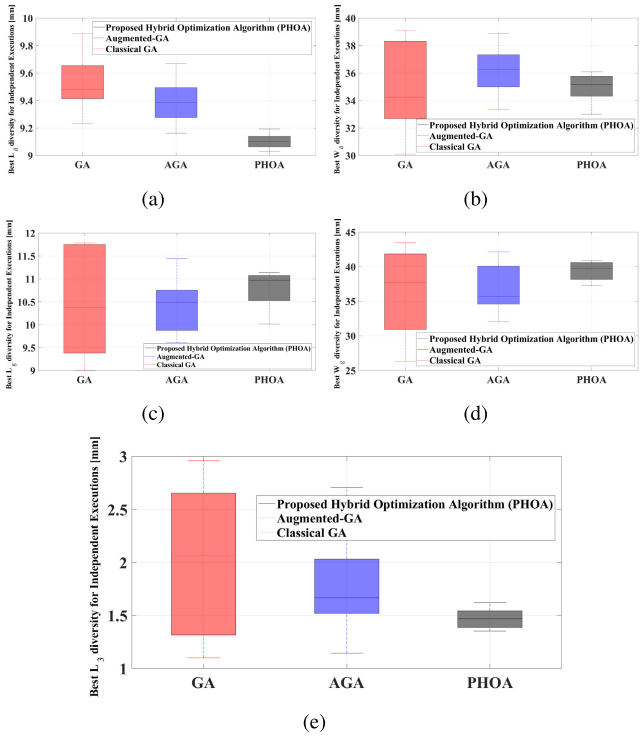

FIGURE 9. Approaching the same results for decision variables in different and independent executions: (a) Optimized L_d results, (b) Optimized W_d results, (c) Optimized L_g results, (d) Optimized W_g results, and (e) Optimized L_3 results.

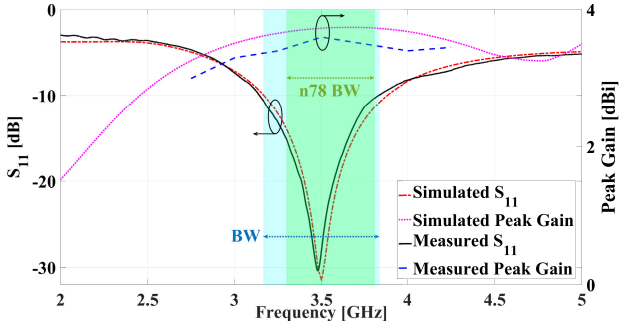

FIGURE 10. The simulated and measured S_{11} and peak gain of the proposed single dipole antenna.

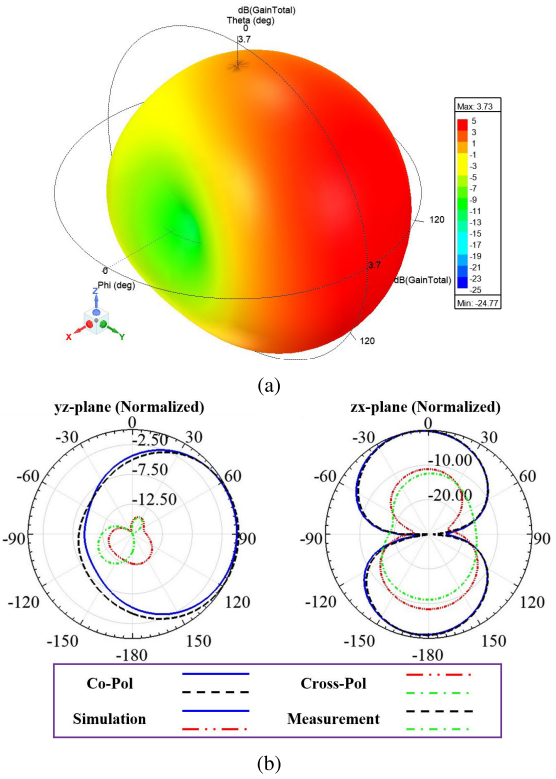

FIGURE 11. 3D and 2D radiation patterns for the proposed antennas at 3.5 GHz: (a) Simulated 3D radiation pattern of the single dipole antenna, and (b) 2D normalized radiation pattern of the single dipole antenna.

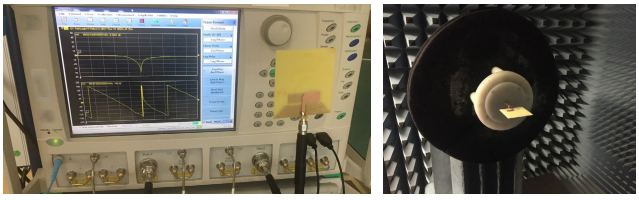

FIGURE 12. Scattering parameters, radiation pattern, and gain measurement setup: (a) Measurement setup for scattering parameters of the single dipole antenna, (b) Measurement setup for radiation pattern and gain of the single dipole antenna.

single-element antenna has 18.79% (3.17-3.83 GHz) IBW which can cover the frequency band of 3.5 GHz for 5G applications. According to Fig. 10, the antenna has a measured peak gain of 3.45 dB in the operating frequency band, and the gain fluctuation in the frequency band is less than 0.3 dB.

Figure 11 displays the simulated and experimental normalized radiation patterns of the single-element antenna in this research. These patterns are plotted in two planes, yz-plane and zx-plane. According to the figure, it can be seen that the antenna has omnidirectional radiation, and its cross-polarization level is at least 10 dB lower than the co-polarization level.

Figure 12 presents the experimental setup for the antenna's scattering, gain, and radiation pattern measurements.

V. PHASE TWO: APPROACH TO THE TARGETED ISOLATION BETWEEN QUAD-MIMO PRINTED DIPOLE ANTENNA ELEMENTS USING PROPOSED HYBRID OPTIMIZATION ALGORITHM

A quad-MIMO antenna was designed using the proposed algorithm and the single-element antenna, which is optimized in section IV so that the isolation between its orthogonal and parallel elements exceeds a specific value. In fact, this antenna is created by placing four radiating elements together, as shown in Fig. 7, with a distance of d_1 from each other. Figure 13 shows the proposed MIMO antenna structure in this paper. This antenna is printed on an FR4 substrate with dimensions of $90\times90\times1.6$ mm^3, loss-tangent of 0.02, and relative permittivity of 4.3. To achieve the maximum amount

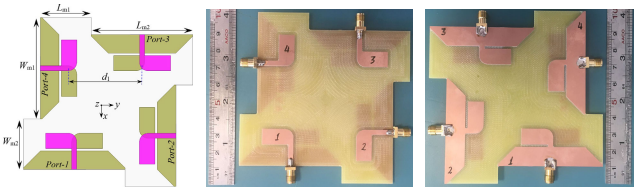

FIGURE 13. The suggested quad-port MIMO dipole antenna: (a) Geometry of the quad-port MIMO antenna, (b) Front-view, and (c) Back-view of the fabricated quad-port MIMO antenna.

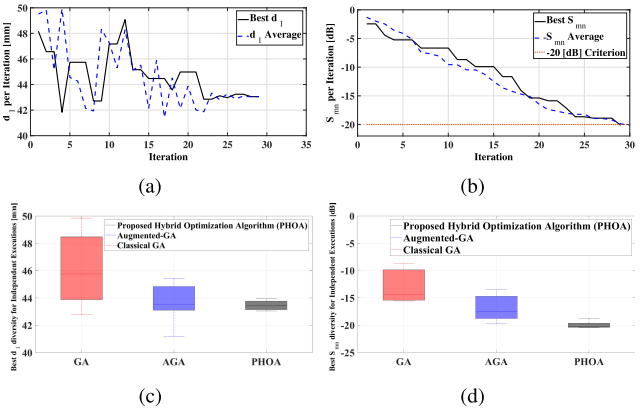

FIGURE 14. Approach and boxplot of decision variable d_1 and isolation S_{mn}: (a) Approaching d_1 to its final value, (b) Approaching S_{mn} to its prespecified target, (c) Optimized d_1 results for independent executions, and (d) Optimized S_{mn} results for independent executions.

of isolation between the adjacent elements of the MIMO antenna, they are positioned orthogonally next to each other. In this way, the radiation element connected to port 1 is perpendicular to the element connected to ports 2 and 4, and it is also parallel to the element connected to port 3. Therefore, MIMO antenna elements are placed together in two distinctive ways: orthogonal (such as ports 1 and 2) and parallel (such as ports 1 and 3). Polarization diversity is created with two adjacent ports by using this method, which improves the isolation of the antenna in orthogonal ports. Also, according to the placement of MIMO antenna elements, it can be seen that although parallel elements have the same polarization, their distance from each other is greater than the distance of orthogonal ones, and this issue can cause improved isolation between parallel elements. Moreover, the minimum distance between parallel and orthogonal antennas, $d_1 = 43.05$ mm, has been determined based on the developed algorithm so that the isolation between them is more than 20 dB.

Figure 14(a) presents the convergence rate and approaching the final goals for the decision variable d_1. The results are obtained for 40 agents/researchers. As is evident from the results, the final goals are attained after around 27 iterations. Figure 14(b) presents the convergence rate and approaching the final goals for the isolation S_{mn}. The results are obtained for 40 agents/researchers. Regarding the average convergence

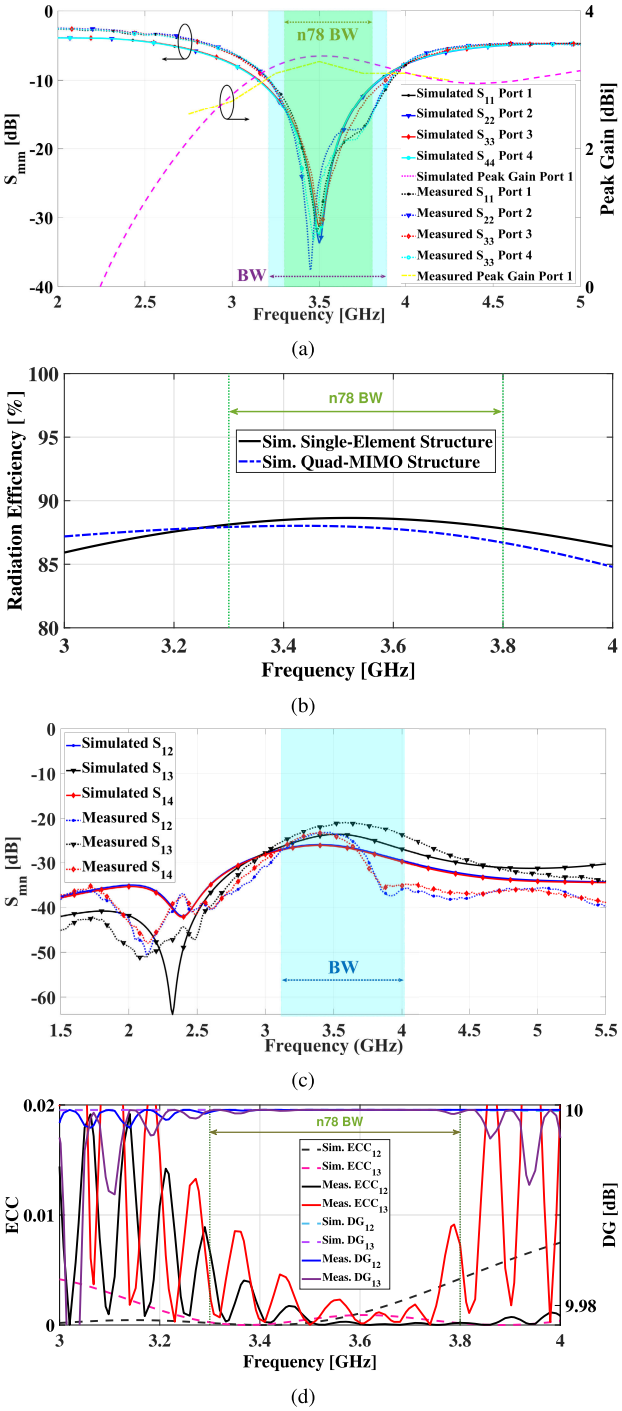

FIGURE 15. The simulated and measured scattering parameters and peak gain: (a) S_{mm} and peak gain of the suggested quad-MIMO dipole antenna, (b) The simulated radiation efficiency for single- and quad-MIMO structure, (c) Isolation results of the orthogonal and aligned elements of the suggested quad-MIMO dipole antenna, and (d) The simulated and measured ECC and DG for suggested quad-MIMO dipole antenna.

rate results, all researchers/agents concentrate on the final target.

The boxplots of the decision variable d_1 for 40 agents/researchers, about 30 iterations, and 10 independent

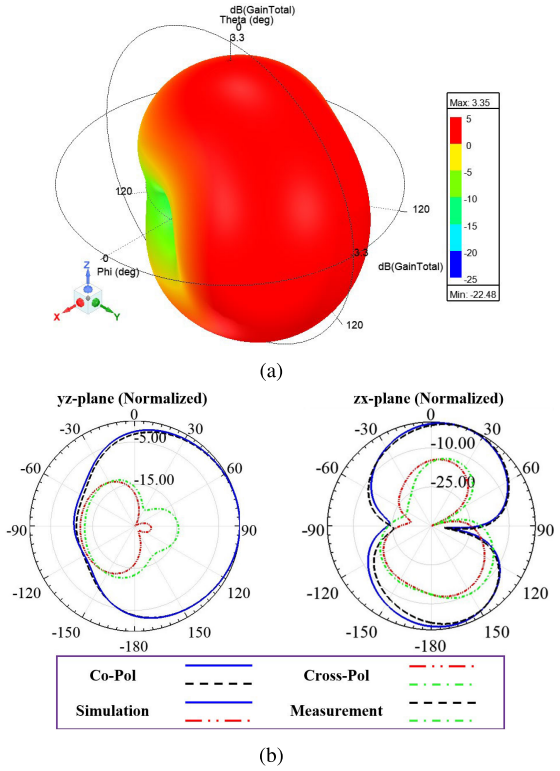

FIGURE 16. 3D and 2D radiation patterns for the suggested antennas at 3.5 GHz: (a) Simulated 3D radiation pattern of the quad-MIMO dipole antenna for Port-1, and (b) 2D normalized radiation pattern of the quad-MIMO dipole antenna for Port-1.

FIGURE 17. Scattering parameters, radiation pattern, and gain measurement setup: (a) Measurement setup for scattering parameters of the quad-port MIMO dipole antenna, (b) Measurement setup for radiation pattern and gain of the quad-port MIMO dipole antenna.

executions are presented in Fig. 14(c) to show the reliability of the proposed hybrid algorithm. The boxplots of the isolation S_{mn} for 40 agents/researchers, about 30 iterations, and 10 independent executions are presented in Fig. 14(d) to show the reliability of the proposed hybrid algorithm. Results prove that the proposed algorithm gives the most reliable results comparing GA and AGA. There is no doubt that more iterations will produce more accurate results, which means more reliability.

The simulated and experimental results of the suggested quad-MIMO antennas' scattering parameters, radiation efficiency, Envelope Correlation Coefficient (ECC), and Diversity Gain (DG) are displayed in Fig. 15. According to the experimental results, the MIMO antenna has an IBW of 19.43% (3.21-3.89 GHz), and all ports show almost the same impedance results, Fig. 15(a). Due to the structural symmetry of the quad-MIMO antenna, only one of its ports has been used to display the antenna's gain, radiation efficiency, and radiation pattern. According to Fig. 15(b), the radiation efficiency for single- and quad-MIMO structures ranges from 86 to 89 percent at the BW. Also, the simulated and experimental isolation results of this quad-MIMO antenna between orthogonal and parallel ports are shown in Fig. 15(c). According to this figure, the isolation between the elements of this antenna is higher than 20 dB. Based on Fig. 15(d), EEC for MIMO structures presents excellent isolation of less than 0.01 at the BW for both orthogonal and parallel elements. In Fig. 15(a), the antenna's simulated and experimental peak gains at port one are compared. The simulated and experimental results in this design agree with each other, and there is a slight difference between them, which is related to the errors in the antenna manufacturing and testing stages. The DG of more than 9.999 presents improved system performance in terms of reliability, coverage, and capacity which leads to better mitigation of fading effects and increased resistance to signal degradation, Fig. 15(d).

In Fig. 16, the comparison of simulation and experimental results of the quad-MIMO antenna radiation pattern for port 1 at 3.5 GHz frequency is reported. The antenna's radiation pattern is relatively stable, and its cross-polarization level is at least 10 dB lower than its co-polarization level.

Figure 17 presents the experimental setup for the suggested quad-MIMO antenna's scattering, gain, and radiation pattern measurements.

VI. CONCLUSION

This study introduces a novel multi-objective hybrid optimization algorithm to enhance antenna electromagnetic properties with prespecified requirements. This algorithm includes merged chaotic maps to make it more reliable and fast. Naturally, the hybrid algorithm combines CM-PSO and an innovative AGA using a uniquely merged chaotic map. Combining algorithms using the implemented method avoided merging difficulties. The ability of the introduced algorithm is evaluated with a single-element dipole and quad-MIMO dipole antenna design. In the first step, a single-element dipole antenna with a 3.5 GHz resonance frequency covering a 3.3 to 3.8 GHz frequency band is designed based on the proposed hybrid algorithm with optimized geometrical values. Then, a quad-MIMO dipole antenna considering less than -20 dB isolation between its elements (criteria) is presented using the optimized single-element dipole antenna to minimize the structure's size. The results prove that the proposed algorithm is appropriate for solving single- and multi-objective problems.

APPENDIX A CHAOTIC MAPS

The Chebyshev Chaotic Map (CCM) is defined as

$$CCM_i(x_{CCM_{i-1}}) = x_{CCM_i} = \left|\cos(i \times \operatorname{acos}(x_{CCM_{i-1}}))\right| \quad (6)$$

$$PCM_j(x_{MCM_{j-1}}, p) = x_{PCM_j} = \begin{cases} \frac{x_{MCM_{j-1}}}{p} & : 0 \le x_{MCM_{j-1}} < p \\ \frac{x_{MCM_{j-1}} - p}{0.5 - p} & : p \le x_{MCM_{j-1}} < 0.5 \\ \frac{1-p - x_{MCM_{j-1}}}{0.5 - p} & : 0.5 \le x_{MCM_{j-1}} < 1-p \\ \frac{1 - x_{MCM_{j-1}}}{p} & : 1-p \le x_{MCM_{j-1}} < 1 \end{cases} \tag{7}$$

in which i is the counter of populations/paired parents/NFE. Then, the Piecewise Chaotic Map (PCM) is defined in Eq. 7, as shown at the top of the page, in which p is set to 0.4 ($p = 0.4$): where j is the NFE. Also, the Iterative Chaotic Map (ICM) is defined as

$$ICM_j(x_{MCM_{j-1}/PCM_{j-1}}) = x_{ICM_j} = |\sin(\frac{a \times \pi}{x_{MCM_{j-1}/PCM_{j-1}}})| \tag{8}$$

in which a is set to 0.9 ($a = 0.9$) and j is the NFE. Finally, the Sinusoidal Chaotic Map (SCM) is defined as

$$SCM_j(x_{ICM_{j-1}}) = x_{SCM_j} = b \times x_{ICM_{j-1}}^2 \times \sin(\pi \times x_{ICM_{j-1}}) \tag{9}$$

in which b is set to 2.3 ($b = 2.3$) and j is the NFE.

REFERENCES

[1] A. Song, W. Chen, T. Gu, H. Yuan, S. Kwong, and J. Zhang, "Distributed virtual network embedding system with historical archives and set-based particle swarm optimization," *IEEE Trans. Syst., Man, Cybern. Syst.*, vol. 51, no. 2, pp. 927–942, Feb. 2021, doi: 10.1109/TSMC.2018.2884523.

[2] Q. Yang, W. Chen, J. D. Deng, Y. Li, T. Gu, and J. Zhang, "A level-based learning swarm optimizer for large-scale optimization," *IEEE Trans. Evol. Comput.*, vol. 22, no. 4, pp. 578–594, Aug. 2018, doi: 10.1109/TEVC.2017.2743016.

[3] S. Khorasani, J. Nourinia, C. Ghobadi, M. Shokri, A. Hatamian, and B. Virdee, "Dual-band magneto-electric dipole antenna with high-gain for base-station applications," *AEU-Int. J. Electron. Commun.*, vol. 134, May 2021, Art. no. 153696, doi: 10.1016/j.aeue.2021.153696.

[4] A. Eslami, J. Nourinia, C. Ghobadi, and M. Shokri, "Four-element MIMO antenna for X-band applications," *Int. J. Microw. Wireless Technol.*, vol. 13, no. 8, pp. 859–866, Oct. 2021, doi: 10.1017/S1759078720001440.

[5] M. Kovaleva, D. Bulger, and K. P. Esselle, "Comparative study of optimization algorithms on the design of broadband antennas," *IEEE J. Multiscale Multiphys. Comput. Techn.*, vol. 5, pp. 89–98, 2020, doi: 10.1109/JMMCT.2020.3000563.

[6] D. E. Kvasov and M. S. Mukhametzhanov, "Metaheuristic vs. deterministic global optimization algorithms: The univariate case," *Appl. Math. Comput.*, vol. 318, pp. 245–259, Feb. 2018, doi: 10.1016/j.amc.2017.05.014.

[7] K. Kaboutari and V. Hosseini, "A compact 4-element printed planar MIMO antenna system with isolation enhancement for ISM band operation," *AEU-Int. J. Electron. Commun.*, vol. 134, May 2021, Art. no. 153687, doi: 10.1016/j.aeue.2021.153687.

[8] K. Kaboutari, A. Zabihi, B. Virdee, and M. P. Salmasi, "Microstrip patch antenna array with cosecant-squared radiation pattern profile," *AEU-Int. J. Electron. Commun.*, vol. 106, pp. 82–88, Jul. 2019, doi: 10.1016/j.aeue.2019.05.003.

[9] M. H. Teimouri, C. Ghobadi, J. Nourinia, K. Kaboutari, M. Shokri, and B. S. Virdee, "Broadband printed dipole antenna with integrated balun and tuning element for DTV application," *AEU-Int. J. Electron. Commun.*, vol. 148, May 2022, Art. no. 154161, doi: 10.1016/j.aeue.2022.154161.

[10] M. Shokri, P. Faeghi, K. Kaboutari, C. Ghobadi, J. Nourinia, Z. Amiri, and R. Barzegari, "A printed dipole antenna for WLAN applications with anti-interference functionality," in *Proc. Photon. Electromagn. Res. Symp. (PIERS)*, Nov. 2021, pp. 1486–1494, doi: 10.1109/PIERS53385.2021.9694670.

[11] M. Shokri, C. Ghobadi, J. Nourinia, P. Pinho, Z. Amiri, R. Barzegari, A. Siahcheshm, F. Shapour, and K. Kaboutari, "A compact four elements self-isolated MIMO antenna for C-band applications," in *Proc. IEEE 27th Workshop Signal Power Integrity (SPI)*, May 2023, pp. 1–4, doi: 10.1109/SPI57109.2023.10145532.

[12] A. Toktas and A. Akdagli, "Compact multiple-input multiple-output antenna with low correlation for ultra-wide-band applications," *IET Microw., Antennas Propag.*, vol. 9, no. 8, pp. 822–829, Jun. 2015, doi: 10.1049/iet-map.2014.0086.

[13] P. Kumar, S. Pathan, S. Vincent, O. P. Kumar, P. Kumar, P. R. Shetty, and T. Ali, "A compact quad-port UWB MIMO antenna with improved isolation using a novel mesh-like decoupling structure and unique DGS," *IEEE Trans. Circuits Syst. II, Exp. Briefs*, vol. 70, no. 3, pp. 949–953, Mar. 2023, doi: 10.1109/TCSII.2022.3220542.

[14] S. Vincent, S. A. J. Francis, K. Raimond, T. Ali, and O. P. Kumar, "An analysis of Metaheuristic algorithms used for the recovery of a failed antenna element in an antenna array," *Int. J. Commun. Antenna Propag. (IRECAP)*, vol. 9, no. 6, p. 409, Dec. 2019, doi: 10.15866/irecap.v9i6.17352.

[15] S. Vincent, S. A. J. Francis, O. P. Kumar, K. Raimond, S. M. Thampi, O. Marques, S. Krishnan, K. Ch Li, D. Ciuonzo, and H. M. Kolekar, "Recovery of a failed antenna element using genetic algorithm and particle swarm optimization for MELISSA," in *Advances in Signal Processing and Intelligent Recognition Systems*. Singapore: Springer, 2019, pp. 217–228, doi: 10.1007/978-981-13-5758-9_19.

[16] D. Ustun, A. Toktas, and A. Akdagli, "Deep neural network-based soft computing the resonant frequency of E-shaped patch antennas," *AEU-Int. J. Electron. Commun.*, vol. 102, pp. 54–61, Apr. 2019, doi: 10.1016/j.aeue.2019.02.011.

[17] G. Singh and U. Singh, "Triple band-notched UWB antenna design using a novel hybrid optimization technique based on DE and NMR algorithms," *Exp. Syst. Appl.*, vol. 184, Dec. 2021, Art. no. 115299, doi: 10.1016/j.eswa.2021.115299.

[18] W. T. Li, X. W. Shi, Y. Q. Hei, S. F. Liu, and J. Zhu, "A hybrid optimization algorithm and its application for conformal array pattern synthesis," *IEEE Trans. Antennas Propag.*, vol. 58, no. 10, pp. 3401–3406, Oct. 2010, doi: 10.1109/TAP.2010.2050425.

[19] Q. Zheng, C. Guo, J. Ding, M. O. Akinsolu, B. Liu, and G. A. E. Vandenbosch, "A wideband low-RCS metasurface-inspired circularly polarized slot array based on AI-driven antenna design optimization algorithm," *IEEE Trans. Antennas Propag.*, vol. 70, no. 9, pp. 8584–8589, Sep. 2022, doi: 10.1109/TAP.2022.3161389.

[20] Z. Bayraktar, P. L. Werner, and D. H. Werner, "The design of miniature three-element stochastic Yagi-Uda arrays using particle swarm optimization," *IEEE Antennas Wireless Propag. Lett.*, vol. 5, pp. 22–26, 2006, doi: 10.1109/lawp.2005.863618.

[21] S. Pattnaik, S. S. Pattnaik, and B. S. Dhaliwal, "Modeling of circular fractal antenna using BFO-PSO-based selective ANN ensemble," *Int. J. Numer. Model., Electron. Netw., Devices Fields*, vol. 32, no. 3, p. e2549, May 2019, doi: 10.1002/jnm.2549.

[22] W. T. Li, L. Xu, and X. W. Shi, "A hybrid of genetic algorithm and particle swarm optimization for antenna design," *PIERS Online*, vol. 4, no. 1, pp. 56–60, 2008.

[23] W. Obaid and A. Hamid, "Optimization of tri-band bow-tie aperture antenna using genetic algorithm and particle swarm optimization," in *Proc. Int. Conf. Eng. Emerg. Technol. (ICEET)*, Oct. 2021, pp. 1–5, doi: 10.1109/ICEET53442.2021.9659639.
[24] V. Hosseini, Y. Farhang, K. Majidzadeh, and C. Ghobadi, "Customized mutated PSO algorithm of isolation enhancement for printed MIMO antenna with ISM band applications," *AEU-Int. J. Electron. Commun.*, vol. 145, Feb. 2022, Art. no. 154067, doi: 10.1016/j.aeue.2021.154067.
[25] V. Hosseini, F. Shapour, P. Pinho, Y. Farhang, K. Majidzadeh, C. Ghobadi, J. Nourinia, S. Barshandeh, M. Shokri, Z. Amiri, M. Jalilirad, and K. Kaboutari, "Dual-band planar microstrip monopole antenna design using multi-objective hybrid optimization algorithm," presented at Proc. Photon. Electromagn. Res. Symp. (PIERS), Jul. 2023.

VAHID HOSSEINI HASBESTAN was born in Urmia, Iran, in 1983. He received the B.Sc. degree in software engineering from Islamic Azad University, Khoy, Iran, in 2006, and the M.Sc. degree in computer software engineering from Islamic Azad University, Shabestar Branch, Iran, in 2010. He is currently pursuing the Ph.D. degree with Islamic Azad University, Urmia Branch, Urmia. Moreover, he is a Payame Noor University Faculty Member with the Department of Computer Engineering and Information Technology, Urmia. His research interest includes computer networking and optimization.

YOUSEF FARHANG was born in Khoy, Iran, in 1978. He received the B.Sc. degree in software engineering from Islamic Azad University, Khoy, in 2001, the M.Sc. degree in software engineering from Islamic Azad University, Arak, Iran, in 2005, and the Ph.D. degree in computer science from Universiti Teknologi Malaysia (UTM), in 2016. He was with Islamic Azad University, Khoy Branch, as a Researcher and a Lecturer, in 2003. His research interests include data mining, clustering algorithm, image clustering, and machine learning algorithms.

KAMBIZ MAJIDZADEH was born in Urmia, Iran, in 1980. He received the B.Sc. degree in software engineering from Islamic Azad University, Khoy, Iran, in 2002, and the M.Sc. degree in computer networking and the Ph.D. degree in information technology from Baku State University (BSU), Azerbayijan, in 2005 and 2009, respectively. Since 2012, he has been working as a Faculty Member at Islamic Azad University, Urmia Branch, Urmia. Presently, he is an Assistant and the Head of the Department of Computer Engineering, Islamic Azad University, Urmia Branch. His research interests include very large-scale integration design, computer networking, and network security.

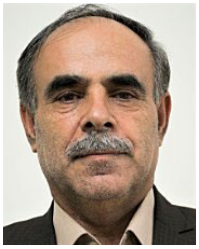

CHANGIZ GHOBADI received the B.Sc. degree in electrical engineering and the M.Sc. degree in electrical engineering telecommunication from the Isfahan University of Technology, Isfahan, Iran, and the Ph.D. degree in electrical telecommunication from the University of Bath, Bath, U.K., in 1998. He is currently a Professor with the Department of Electrical Engineering, Urmia University, Urmia, Iran. He has supervised and administered more than 130 M.Sc. and 32 Ph.D. students and their thesis. He has authored or coauthored over 360 scientific publications including accredited journals and conferences. His articles have been cited over 5750 times. His research interests include antenna design, radar, and adaptive filters. He has been included at the Top 1% of the World's Scientists and Academics according to Thomson Reuters' list, in 2017, 2020, and 2022.